(Preprint) AAS 23-219

LEVERAGING THE GROUND-TRACK RESONANCE CAPTURE AND ESCAPE FOR PRECISE AND EFFICIENT ORBITAL TRANSFERS

Wail Boumchita[*] and Jinglang Feng[†]

Vesta, the second largest celestial object in the main asteroid belt, was visited and studied by the Dawn mission in 2011. The spacecraft employed solar-electric propulsion, which generated continuous low-thrust. During the slow descent from high altitude mission orbit (HAMO) to low altitude mission orbit (LAMO), the spacecraft encountered the 1:1 ground-track resonance, with the potential of being captured and trapped in it. The objective of this paper is to present a workflow for designing orbit transfers from HAMO to LAMO by leveraging the effects of the 1:1 ground-track resonance, achieved only by adjusting the thrust magnitude value throughout the descent. Firstly, the dynamics are modeled by considering the irregular gravitational field up to the fourth order and degree, while the thrust remains constant in magnitude and opposes the velocity direction of the spacecraft. Subsequently, a reference case of capture into the 1:1 ground-track resonance is considered, and the effects of the resonance on the trajectory of the spacecraft are described. Following that, the workflow adopted for designing orbit transfers during Dawn's approach phase is presented, and a case study is conducted to apply the workflow. This paper contributes to raising awareness regarding the risk of resonance capture and highlights strategies for escaping such resonances, thereby facilitating the design of future space missions to asteroids.

INTRODUCTION

Resonance is a widespread concept in dynamical systems, occurring when a system is driven at its natural frequency, leading to pronounced oscillations. Its manifestations cut across various fields, from plasma physics[1] to celestial mechanics[2] and astrodynamics[3] . Within the context of celestial mechanics and astrodynamics, numerous types of orbital resonances can be observed. These include mean motion resonances[4] , where the orbital periods of two bodies have a simple integer ratio; secular resonances[5] , which affect the long-term evolution of orbits; secondary resonances[6] , which are combinations of simpler resonances; spin-orbit resonances,[7] where a body's rotational period and orbital period are linked; and ground-track resonances (GTRs),[3] where the gravitational effects of bodies influence each other's orbits. For GTRs to occur, the period of revolution of the spacecraft has to be commensurable to the period of rotation of the asteroid around its axis. For example, in the 1:1 GTR the revolution period of the spacecraft is equal to the rotation period of the Earth around its spin axis[8] , as in the case of spacecraft in GEO.

[*]wail.boumchita@strath.ac.uk, Ph.D. Student, Department of Mechanical and Aerospace Engineering, University of Strathclyde, Glasgow, G1 1XJ, UK

[†]jinglang.feng@strath.ac.uk, Lecturer, Department of Mechanical and Aerospace Engineering, University of Strathclyde, Glasgow, G1 1XJ, UK

In 2011, the spacecraft Dawn successfully approached the asteroid Vesta.[9] The Dawn mission was one of the first missions to use low-thrust propulsion during both the cruise phase and the approach phase to an asteroid. It demonstrates the possibility of relying on low-thrust propulsion for the majority of the mission duration[10,11] . As the spacecraft slowly approaches the asteroid, there is a possibility that it is captured by the 1:1 GTR and permanently trapped in it.[3] The spacecraft at each revolution encounters the same gravitational configuration, the effect of which accumulates over the revolutions and change noticeably the orbit eccentricity and inclination. Small variations in the initial state of the spacecraft can make a difference in whether the spacecraft manages to cross the resonance and reach lower altitudes if the spacecraft remains trapped in the resonance despite the continuous thrusting. Tricarico and Sykes[3] and Delsate[12] studied in depth the phenomenon of capture into 1:1 GTR. The awareness that the mission was potentially in danger due to the 1:1 GTR was brought by the former, which estimated the probability of capture. The latter further refined the previous study by updating the estimate of the probability of capture into the 1:1 GTR, thereby offering additional information on the phenomenon and presenting a general methodology for searching and analytically locating the main resonances. Delsate concluded his study by considering the possibility of escaping from the resonance and highlighting the dependence of this possibility on the phase of the resonance angle.

For this research, the previous investigation is extended to advance the knowledge of resonance escape by analyzing the possibility of escaping from the 1:1 GTR around Vesta solely through an increase in the thrust magnitude. Orbital transfers can be achieved in two ways: impulsive maneuvers or continuous low-thrust maneuvers. Given that Dawn was equipped with a low-thrust propulsion system, the approach was performed using continuous low-thrust. In previous studies[13] , the descent was analyzed by leveraging GTRs and controlling the thrust through the activation and deactivation of its magnitude and direction. In the course of satellite mission planning and operation, the implications of frequent spacecraft maneuvers warrant careful consideration, given the cumulative negative effects such actions often yield. One significant drawback is the inherent uncertainty introduced with each maneuver, which can potentially compound over time, thereby augmenting trajectory deviation and instigating a cascade of subsequent course corrections. This can lead to a recursive cycle of corrections and uncertainties, ultimately creating a more complex operational scenario. From a hardware perspective, the persistent utilization of thrusters intensifies their wear and tear, thereby reducing their overall lifespan and potentially compromising their performance. On the other hand, in this work, the number of times the thrust magnitude value is changed throughout the descent is limited, and the thrust is kept constantly aligned with the direction of the spacecraft's velocity.

This work is structured as follows: the equations of motion and the Hamiltonian dynamical model are defined. The phase-space of the model is obtained, providing important insights into the phenomenon of resonance. Then, the analysis focuses on the effects of the 1:1 GTR on the descent trajectory of Dawn, specifically on how the accumulation of gravitational perturbation affects the evolution of the semimajor axis, inclination (i), and longitude of the ascending node (Ω). Subsequently, the rationale and the workflow for designing the transfer orbits are presented. The workflow is then applied to a case study, wherein an orbit transfer from HAMO to LAMO is designed, leveraging the 1:1 GTR. Finally, the study concludes with the final section.

DYNAMICAL MODELING

In this section, the dynamical environment surrounding Vesta is investigated to identify perturbations that need to be considered for the modeling of the dynamics. Subsequently, Vesta's physical

and gravitational characteristics and the equations of motion for the spacecraft are presented. The Hamiltonian function of the system is then defined and the dynamics of the Dawn mission phase-space are investigated.

Main perturbations

In 2011, the Dawn spacecraft successfully arrived at the asteroid Vesta. During the approach phase, the spacecraft descended from a high-altitude mission orbit (HAMO) to a low-altitude mission orbit (LAMO) utilizing low-thrust propulsion. The orbital radii of the HAMO and LAMO are 1000 km and 460 km, respectively.[3] However, the use of low-thrust propulsion during the descent phase posed a risk of capturing the spacecraft into GTRs around Vesta. The physical parameters of Vesta are listed in Table 1, and it is assumed to rotate uniformly around a constant direction in the inertial frame. The unnormalized Stokes coefficients of Vesta are given in Feng[14] .

Table 1: Vesta's physical parameters[3]

Gravitational constant	μ	17.5 km^3/s^2
Reference radius	R_e	300 km
Angular velocity	ω	3.2671×10^{-4} rad/s

The spacecraft is subject to the following perturbations:[15]

- Vesta's irregular gravitational perturbations

$$a_{nm} = (n+1)\frac{\mu}{r^2}\frac{R_e^n}{r^n}J_{nm}$$

  where $J_{nm} = \sqrt{C_{nm}^2 + S_{nm}^2}$;

- Sun's gravitational perturbation

$$a_{Sun} = \frac{2\mu_{Sun}}{d_{Sun}^3}r$$

- solar radiation pressure perturbation

$$a_{SRP} = C_r\frac{A}{m}P_\odot$$

where r represents the distance from the spacecraft to Vesta, C_{nm} and S_{nm} are the unnormalized Stokes coefficients, n and m are the degree and order of the spherical harmonic expansion considered, $\mu_\odot$ represents the gravitational constant of the Sun, $d_\odot$ is the distance of the spacecraft from the Sun, $C_r = 0.25$ is the reflectivity coefficient of the spacecraft, $A/m = 0.04$ is the area-to-mass ratio of the spacecraft, and $P_\odot$ is the solar radiation pressure at a distance $d_\odot$ from the Sun. The magnitudes of the main perturbations at different orbital radii are illustrated in Figure 1. A thorough analysis of the figure reveals that at the orbital radius corresponding to the 1:1 GTR, i.e. 550 km, Vesta's gravitational perturbations are an order of magnitude stronger than the perturbations from the Sun's gravitational attraction, and the solar radiation pressure. This highlights the importance of accurately accounting for Vesta's gravitational influence in the dynamic modeling of the

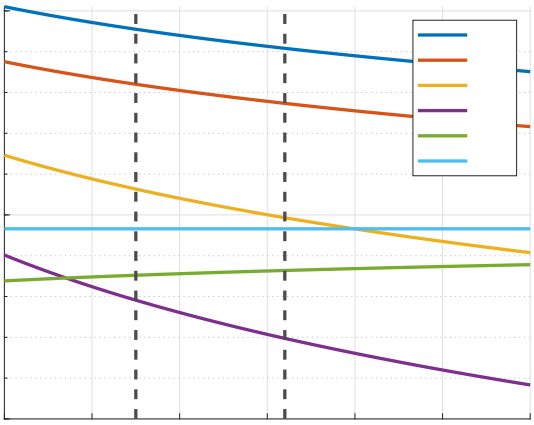

Figure 1: Order of magnitude of the various perturbations to which the Dawn spacecraft is subject at different orbital radii. The location of the 1:1 and 2:3 GTRs are highlighted for reference.

spacecraft's trajectory. Furthermore, it is worth noting that the relative magnitudes of these perturbations can vary significantly depending on the orbital radius of the spacecraft. Given the dominant effect of Vesta's irregular gravitational perturbations at the 1:1 GTR and the potential impact on the spacecraft's trajectory, in this paper, only these perturbations are considered in the dynamical modeling.

Equations of motion

The model considered is the perturbed two-body problem with perturbations from the irregular gravitational field of Vesta and the low-thrust to which the spacecraft is subject. Tricarico[3] has proved that with a spherical harmonic expansion up to the 8^{th} order, the dynamics is dominated by the 3^{rd} and 4^{th} order terms. Therefore, the gravitational field truncated to the fourth order and degree is used. The low-thrust is constant in magnitude and it always in the opposite direction of Dawn's velocity.

Kaula[16] defined the gravitational potential of a central body as a function of the spherical harmonics. The characteristics of the asteroid including the shape and volume density variations are taken into account through the Stokes coefficient. The gravitational field V of degree n and order m in spherical harmonics expansion is given in spherical coordinated (r,δ,ϕ) as

$$V = \frac{\mu}{r} + \sum_{n=2}^{\infty} \sum_{m=0}^{n} \frac{\mu}{r} \left(\frac{R_e}{r}\right)^n P_{nm}(\sin\phi)(C_{nm}\cos m\delta + S_{nm}\sin m\delta) \tag{1}$$

where δ and ϕ are the colatitude and the longitude respectively. Previous studies have shown that the dynamics around Vesta are primarily influenced by the spherical harmonics expansion up to the 4th order and degree.[3] This is also the truncation order adopted in our current study. Our simulations focus on the perturbed two-body problem,[13] where the spacecraft is subject to perturbations from Vesta's irregular gravitational field and a constant low-thrust force in the opposite direction of the

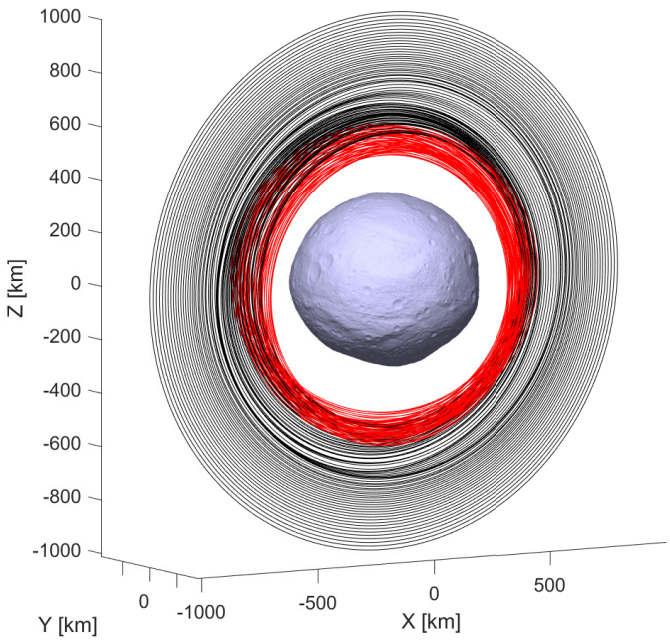

Figure 2: Sample of a trajectory captured into resonance with Vesta. The black line represents the first part of the descent, the red line represents the trajectory after the capture occurs.

spacecraft's velocity. The equations of motion in cartesian coordinates and in the asteroid's centered inertial frame are

$$\begin{cases} \ddot{\mathbf{x}} & = \nabla V - \frac{T}{m(t)}\hat{\mathbf{v}} \\ \dot{m} & = -\frac{T}{I_{sp} g_0} \end{cases} \tag{2}$$

where $\mathbf{x} = [x, y, z]$ is the position vector in cartesian coordinates, $\ddot{\mathbf{x}} = [a_x, a_y, a_z]$ is the acceleration vector, V represents the potential in spherical harmonics in Equation 1, T is the thrust magnitude, m is the spacecraft's mass and $\hat{\mathbf{v}}$ is the spacecraft's velocity unit vector. Finally, the second equation describes the rate of change of the spacecraft's mass over time as a function of I_{sp} and g_0 which represent the specific impulse and Earth's gravitational constant respectively. The equation of motion are propagated using the MATLAB built-in function `ode113` which is a variable-step, variable-order Adams-Bashforth-Moulton solver of orders 1 to 13,[17] with a relative and absolute tolerance set at 10^{-12}. Figure 2 shows a sample of a trajectory captured into resonance in the asteroid's centered inertial frame.

The Hamiltonian formalism is an effective method for analyzing resonance dynamics. The gravitational field, as defined in Equation 1, can be represented as a function of orbital elements, as[16]

$$V = \frac{\mu}{r} + \sum_{n=2}^{\infty} \sum_{m=0}^{n} \sum_{p=0}^{n} \sum_{q=-\infty}^{\infty} \frac{\mu R_e^n}{a^{n+1}} F_{nmp}(i) G_{npq}(e) S_{nmpq}(\omega, M, \Omega, \theta) \tag{3}$$

where $F_{nmp}(i)$ and $G_{npq}(e)$ are functions of the inclination i and eccentricity e, respectively, ω represents the argument of periapsis, M is the mean anomaly, Ω denotes the longitude of the ascending

node, θ represents the sidereal time, and n, m, p, q are integers and

$$S_{nmpq} = \begin{cases} C_{nm}\cos\Psi_{nmpq} + S_{nm}\sin\Psi_{nmpq}, & \text{if } n-m \text{ is even} \\ -S_{nm}\cos\Psi_{nmpq} + C_{nm}\sin\Psi_{nmpq}, & \text{if } n-m \text{ is odd} \end{cases}$$

where Ψ_{nmpq} is the Kaula's phase angle that is defined as

$$\Psi_{nmpq} = (n-2p)\omega + (n-2p+q)M + m(\Omega-\theta). \tag{4}$$

GTRs occur when the rate of change of Kaula's phase angle $\dot{\Psi}_{nmpq}$ is close to zero or when the phase angle of the system remains relatively constant over time.

By defining the quantity $L = \sqrt{\mu a}$ as the conjugate momentum to $\lambda = M + \Omega + \omega$, the Hamiltonian that describes the motion of the spacecraft around an asteroid with an irregular gravitational field can be defined as

$$\mathcal{H} = -\frac{\mu^2}{2L^2} + \sum_{n=2}^{\infty}\sum_{m=0}^{n}\sum_{p=0}^{n}\sum_{q=-\infty}^{\infty} R_e^n \frac{\mu^{n+2}}{L^{2n+2}} F_{nmp}(i) G_{npq}(e) S_{nmpq}(\omega, M, \Omega, \theta) + \dot{\theta}\Lambda \tag{5}$$

where Λ is the conjugated momentum to the sidereal time θ and the term $\dot{\theta}\Lambda$ accounts for the asteroid's rotation. The dynamics of the system close to the 1:1 GTR are primarily affected by the gravitational term up to the second degree and order.[18] In light of this, the Hamiltonian used in the analysis is limited to the second order and degree. The harmonic contributions incorporated in the potential V are selected based on the resonance under consideration. In the case of the 1:1 GTR, the harmonics that contribute to this resonance are listed in Table 2.

Table 2: Spherical harmonics terms related to the 1:1 GTR up to 2nd order and degree ($e = 0$)[16]

n	m	p	q	Ψ_{nmpq}	F_{nmp}	G_{npq}
2	0	1	0	0	3/4 $\sin^2 i$ - 1/2	1
2	2	0	0	$2\lambda - 2\theta$	$3(1+\cos i)^2/4$	1

For a polar circular orbit, the Hamiltonian is

$$\mathcal{H}_{1:1} = -\frac{\mu^2}{2L^2} + \frac{1}{4}R_e^2\frac{\mu^4}{L^6}C_{20} + \frac{3}{4}R_e^2\frac{\mu^4}{L^6}\sqrt{C_{22}^2+S_{22}^2}\cos\left[\Psi_{2200} + \arctan\left(-\frac{S_{22}}{C_{22}}\right)\right] + \dot{\theta}\Lambda \tag{6}$$

where the first argument of the cosine is

$$\Psi_{2200} = 2(\omega + M + \Omega) - 2\theta = 2(\lambda - \theta). \tag{7}$$

The resonance angle σ in the case of 1:1 GTR is

$$\sigma = \lambda - \theta \tag{8}$$

However, in order to preserve a set of canonical variables, it is necessary to perform a canonical transformation. These transformations are important in Hamiltonian mechanics as they allow for

Table 3: Dawn's nominal initial conditions at HAMO[3]

Mass	m	1000 kg
Thrust magnitude	T	20 mN
Specific impulse	I_{sp}	3000 s
semimajor axis	a_0	1000 km
Eccentricity	e_0	0
Inclination	i_0	90°
Longitude of the ascending node	Ω_0	0°
Argument of periapsis	ω_0	0°
True anomaly	θ_0	72°

the definition of new variables that can simplify the analysis of the Hamiltonian function. In this particular case, the canonical transformation proposed by Valk[19] is adopted. The new set of variables is

$$\sigma \quad , \quad L' = L \quad , \quad \theta' = \theta \quad , \quad \Lambda' = \Lambda + L.$$

As a result of this transformation, the new Hamiltonian is

$$\tilde{\mathcal{H}}_{1:1} = -\frac{\mu^2}{2L^2} - \frac{1}{4}R_e^2\frac{\mu^4}{L^6}C_{20} - \frac{3}{4}R_e^2\frac{\mu^4}{L^6}\sqrt{C_{22}^2 + S_{22}^2}\cos\left[2\sigma + \arctan\left(-\frac{S_{22}}{C_{22}}\right)\right] - \dot{\theta}L \quad (9)$$

in which the prime signs are dropped for simplicity and the constant $\dot{\theta}\Lambda'$ term is not included since the expression is no more explicitly dependent on θ. For Vesta, $S_{22} = 0$, so the Hamiltonian is simplified as

$$\tilde{\mathcal{H}}_{1:1} = -\frac{\mu^2}{2L^2} - \frac{1}{4}R_e^2\frac{\mu^4}{L^6}C_{20} - \frac{3}{4}R_e^2\frac{\mu^4}{L^6}C_{22}\cos 2\sigma - \dot{\theta}L. \quad (10)$$

CAPTURE INTO 1:1 GTR

The 1:1 GTR is one of the major resonances that Dawn goes through during its slow descent from HAMO to LAMO. In particular, it is the resonance with greater amplitude.[12] The location of the 1:1 GTR depends on the initial inclination and eccentricity of the descent trajectory and the condition to locate it is

$$\frac{\partial\tilde{\mathcal{H}}_{1:1}}{\partial L} = \frac{\partial\tilde{\mathcal{H}}_{1:1}}{\partial\sigma} = 0 \quad (11)$$

from which the following solutions are obtained

$$\sigma_{st} = 0 \quad , \quad \sigma_{st} = \pi \quad , \quad \sigma_{un} = \pi/2 \quad , \quad \sigma_{un} = 3/2\pi. \quad (12)$$

These equilibrium points are the locations in the phase-space where the spacecraft's motion is stationary in the body-fixed frame.[20] Figure 3 shows the phase-space of the 1:1 GTR from Equation 10, where the stable and unstable equilibrium points are indicated with a triangle and a cross, respectively. The region of interest, also known as the resonance region, is confined between the two red curves, called separatrices. The regions above and below the resonance region are referred to as the upper and lower circulation region, respectively. The initial conditions are reported in Table 3.

From Equation 11, it can also be determined that the location of the 1:1 GTR is approximately 550 km. Therefore, in case the spacecraft is captured into 1:1 GTR around Vesta the radial distance oscillates around the resonance location as in Figure 4.

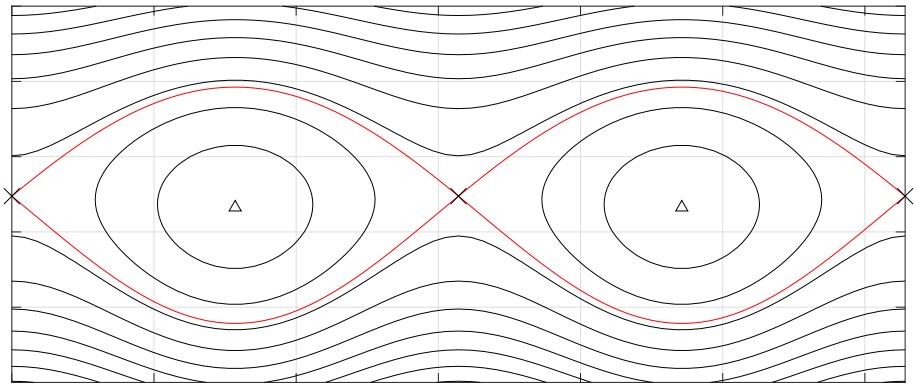

σ

Figure 3: Phase-space configuration of the 1:1 GTR around Vesta. The black curves are the different energy levels, while the red lines are the separatrices that enclose the two resonance regions. The stable and unstable equilibrium points are indicated with a triangle and a cross, respectively.

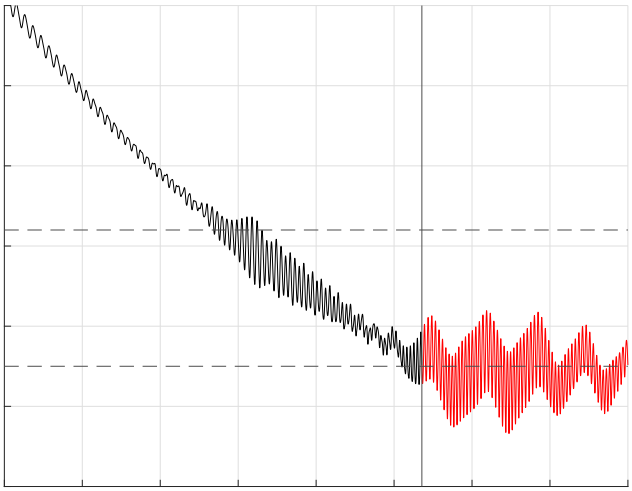

Figure 4: The radial distance evolution with respect to time in the case of the spacecraft being captured into 1:1 GTR with Vesta. The vertical line indicates the time epoch of the resonance capture.

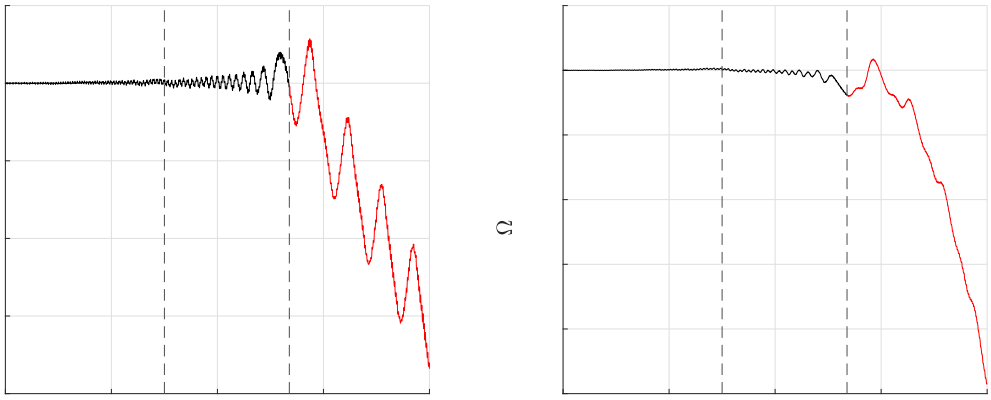

Figure 5: The inclination (on the left) and the Ω (on the right) evolution with respect to time in the case of the spacecraft being captured into 1:1 GTR with Vesta. The vertical line indicates the 2:3 and 1:1 GTR crossing and the red lines indicate the evolution of the parameters inside the 1:1 GTR.

The resonance amplifies the gravitational perturbations on the motion of the spacecraft and acts on the orbital parameters of the trajectory. The consequences of such an accumulation of perturbations cause the excessive need for corrective maneuvers or, in the worst case, deviate the spacecraft from its nominal trajectory, causing it to impact the surface of the asteroid. In particular, the inclination oscillates and the average value of the oscillations decreases linearly. In 13 days within the 1:1 GTR, the inclination decreases by approximately 7° as in the left plot of Figure 5. The Ω evolution follows qualitatively the same trend as its average value remains constant over time and, as the spacecraft crosses the 1:1 GTR, it value begins to decrease without the large oscillations to which the inclination was subject to as shown in the right plot of Figure 5.

ESCAPE FROM 1:1 GTR

The accumulation of perturbations from the GTRs could lead the spacecraft into an unstable orbit, resulting in the impact of the surface of the central body or redirection into a trajectory beyond the gravitational influence of the central body. If there is no interest in leveraging the effect of the GTRs, it is recommended to escape from the resonance as soon as possible and to adjust the trajectory after crossing it through correction maneuvers. It has been shown by Boumchita and Feng[21] that after escaping the GTR, the average value of inclination remains constant with slight oscillations, indicating the potential to exploit GTRs for efficient and precise plane change maneuvers, resulting in propellant savings. The dependence of resonance escape on the phase angle of the escape maneuver is emphasized by Delsate,[12] and Boumchita and Feng[21] conducted a sensitivity analysis on the escape maneuvers required to escape from the 1:1 GTR using only thrust magnitude change maneuvers. It is found that the escape is more effective when the maneuvers are performed near the lower separatrix.

During the escape maneuver, it is interesting to analyze the change in the inclination value between the value at escape and the final value at LAMO. Figure 8 illustrates the absolute difference between the initial and final inclination values, where the initial conditions are obtained when the escape maneuver from the 1:1 GTR is executed, and the final value is taken once the trajectory

reaches a semimajor axis value of 400 km. A smaller difference indicates a more precise maneuver. The range of thrust magnitude values extends from 20 mN (no increase in thrust magnitude from the initial descent) to 49 mN. Nevertheless, this analysis is performed considering a maximum thrust magnitude of 60 mN. The successful escape maneuvers are represented by the red points, while the failed escape maneuvers are represented by the blue points in the figure. It is observed that the first successful escape cases commence by increasing the thrust magnitude to 22 mN as soon as the spacecraft is captured into resonance, and as the thrust magnitude is further increased, the number of successful cases also rises. If the capture continues for a longer time interval, a higher thrust magnitude is required to escape the resonance. Additionally, in all cases where the spacecraft successfully escapes from the resonance, the absolute difference between the initial and final inclination values is small. Conversely, for the cases in which the spacecraft fails to escape from the resonance, the inclination values continue to evolve, resulting in a large Δi.

WORKFLOW

The semimajor axis, inclination, and Ω are primarily perturbed by the 1:1 GTR. Upon being captured into 1:1 GTR with Vesta, the semimajor axis undergoes oscillations around the resonance location. Throughout the descent, the average value of the inclination remains constant, and upon capture into resonance, its value begins to oscillate while decreasing almost linearly over time. Similarly, the Ω value remains constant before the capture but decreases when the capture occurs.

The inputs required for designing the orbit transfer are the final orbit geometry, specified in terms of semimajor axis, inclination, and Ω, as well as the magnitude of thrust change necessary to escape from the resonance. The output is the orbit transfer within the 1:1 GTR, utilizing the gravitational perturbations from Vesta to effect the changes in inclination and Ω. After achieving the desired geometry, the thrust is increased from 20 mN to the magnitude of thrust required for escaping from the resonance.

The workflow used in this paper is schematized in Figure 7.

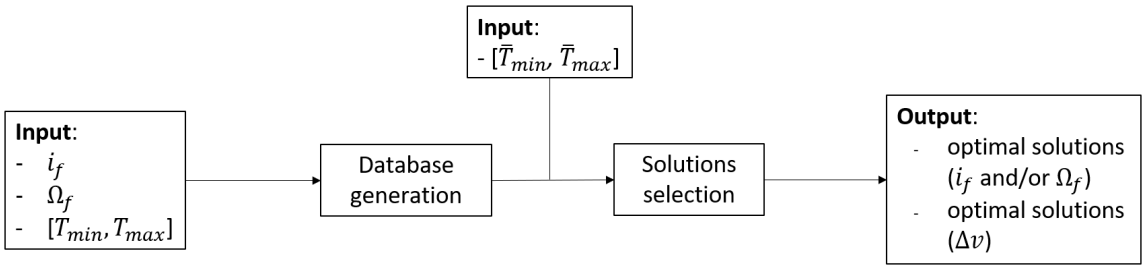

Figure 7: Overall pipeline of the framework.

Once the final geometry and the available thrust magnitude are defined, the given constraints are used to extract all the solutions from a database of all possible solutions, which is generated a priori. The database is generated by considering the same initial condition from the descent (specify initial conditions). After selecting the solutions, their orbital parameter evolution over time is propagated and plotted. Subsequently, one variable to be optimized, either Δv, i, or Ω, is defined. Finally, the selected solution is propagated and displayed.

The database of possible solutions is created by propagating trajectories, with initial conditions

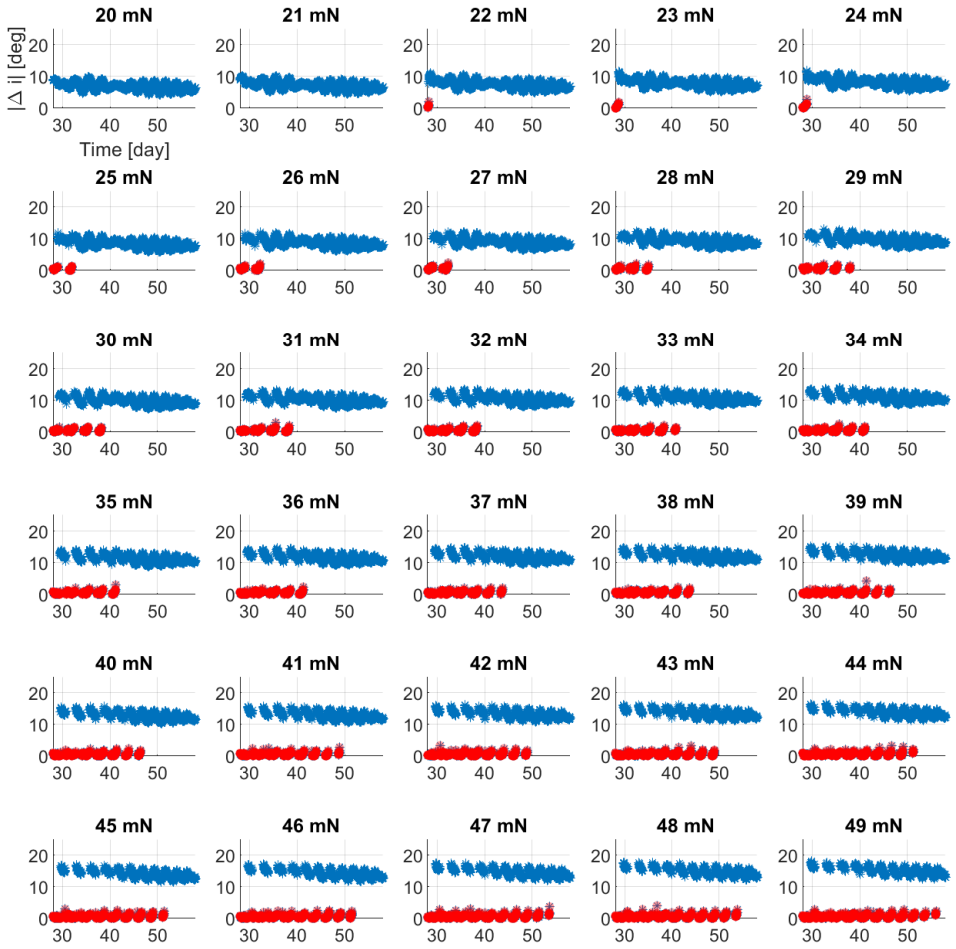

Figure 6: The difference between the initial and final values of the inclination. The cases in which the spacecraft escapes from the resonance and the cases in which it fails are highlighted in red and blue respectively.

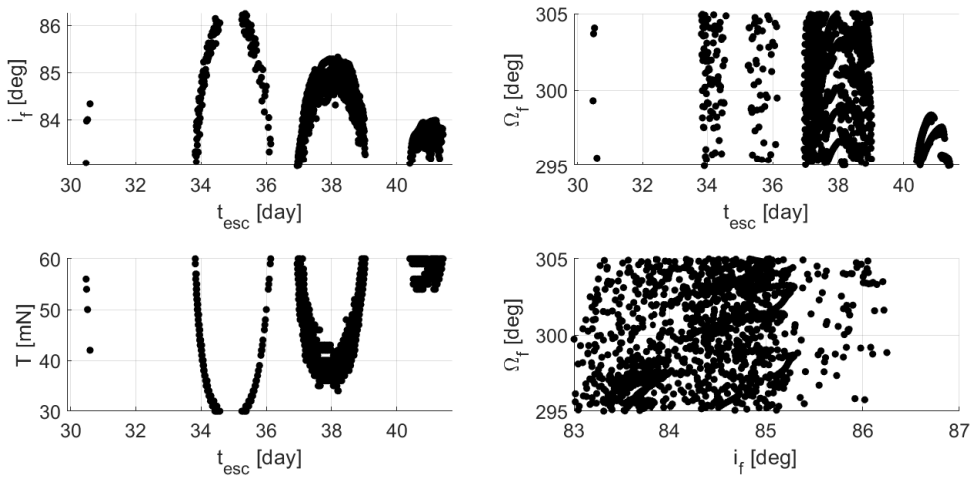

Figure 8: Maps of the acceptable solutions distribution. The upper plot show the distribution in terms of final inclination and Ω respectively. The lower plots show the distribution as a function of the thrust magnitude values (on the left) and as a function of final inclination and Ω (on the right).

inside the 1:1 GTR. For each initial condition, the minimum thrust magnitude change is identified, and the final values of the orbital elements are saved. We consider 1000 different initial conditions after the spacecraft has been captured inside the resonance for 30 days, and the thrust magnitude range extends from 21 to 92 mN.

The use of maps provides a visual representation of all possible solutions, providing insights into the distribution of feasible solutions over the time interval. It also reveals the number of solutions and their distribution for each value of thrust magnitude, as well as the conditions that impose greater strictness. Moreover, an analysis is conducted to determine if these conditions can be relaxed or not. Additionally, these maps can be utilized to optimize the tolerances of the desired final solutions.

CASE STUDY

In this section, an orbital transfer from HAMO to LAMO is achieved using the workflow described in the previous section. The initial conditions at HAMO are listed in the first column of Table3. The spacecraft is directed toward the resonance with the intention of being captured in it. The desired final conditions are also set a priori in terms of semimajor axis, inclination, and Ω and, in this case, are set to $a = 400$km, $i_f = 85^\circ \pm 2^\circ$ and $\Omega_f = 300^\circ \pm 5^\circ$. The thrust magnitude values considered are included in the interval [30, 60] mN. The thrust magnitude interval chosen for this case study is arbitrary. The workflow can be expanded by considering a range of thrust magnitudes up to the maximum value available. Since the aim of this paper is to design orbit transfers that optimize fuel consumption, the restricted interval [30, 60] mN is considered.

The different maps that are used to design the escape trajectory are shown in Figure 8. After the final conditions and their respective tolerances have been fixed, the initial conditions that satisfy those conditions are plotted. The upper plots depict the distribution of the acceptable cases over the escape time in terms of final inclination and Ω, respectively. The lower left plot illustrates the distribution of those solutions across different values of thrust magnitude. Lastly, the lower right plot displays the distributions of the solutions in terms of the final geometry, which is useful for

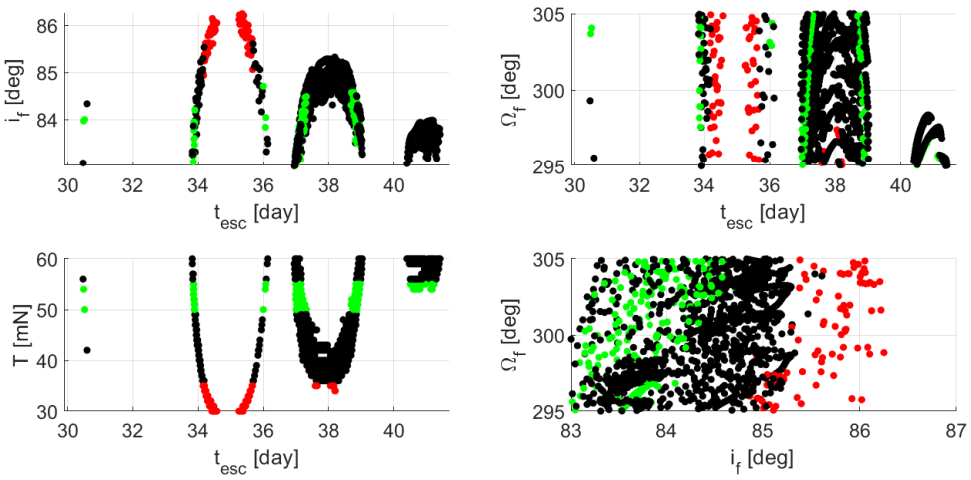

Figure 9: Maps of the acceptable solutions distribution. The upper plot show the distribution in terms of final inclination and Ω respectively. The lower plots show the distribution as a function of the thrust magnitude values (on the left) and as a function of final inclination and Ω (on the right). The solution which are obtained from the thrust interval [30,35] mN and [50,55] mN are highlighted in red and green respectively.

selecting a subset of the acceptable solutions.

Two subsets of acceptable solutions are displayed in Figure 9 after fixing the value of thrust values. The solutions for T = [30,35] mN and T = [50,55] mN are highlighted in red and green, respectively. The final values of Ω are evenly distributed among the solutions with low thrust magnitudes, and they are concentrated in the upper part of the final inclination interval. In contrast, the solutions with high-thrust magnitudes are concentrated in the lower part of the final inclination interval. The evolutions over time of the semimajor axis, eccentricity, inclination, and Ω for all the acceptable solutions (in grey) are displayed in Figure 10. Among all the solutions, the optimal solution can be chosen in terms of final inclination (in red) and optimal Δv (in green). The desired inclination and Ω values are represented by the black dashed line, and the tolerances on those values are constrained by the red dashed lines in the lower plots.

The evolutions of the semimajor axis, inclination, and Ω from HAMO to LAMO are shown in Figure 11. The descent is initiated from 1000 km, leading to a decrease in the semimajor axis value, while the inclination and Ω remain approximately constant, except for small oscillations. After 27 days, the spacecraft is captured into 1:1 GTR, and the semimajor axis oscillates around the location of the resonance, i.e. 550km. Over time, the amplitude of inclination value oscillations increases, and the average value linearly decreases. Additionally, the value of Ω decreases as time progresses. After 38 days, the first maneuver is performed by increasing the value of the thrust magnitude to 35 mN, enabling the trajectory to escape from the resonance. As the spacecraft departs from the resonance, the semimajor axis value decreases until the 400 km mark value is reached. The inclination value oscillates while maintaining an approximately constant average value, and the Ω value continues to decrease. Once the semimajor axis reaches the altitude of LAMO, the thrust is deactivated. Consequently, the average values of the semimajor axis and inclination remain constant, while the average value of Ω continues to decrease over time.

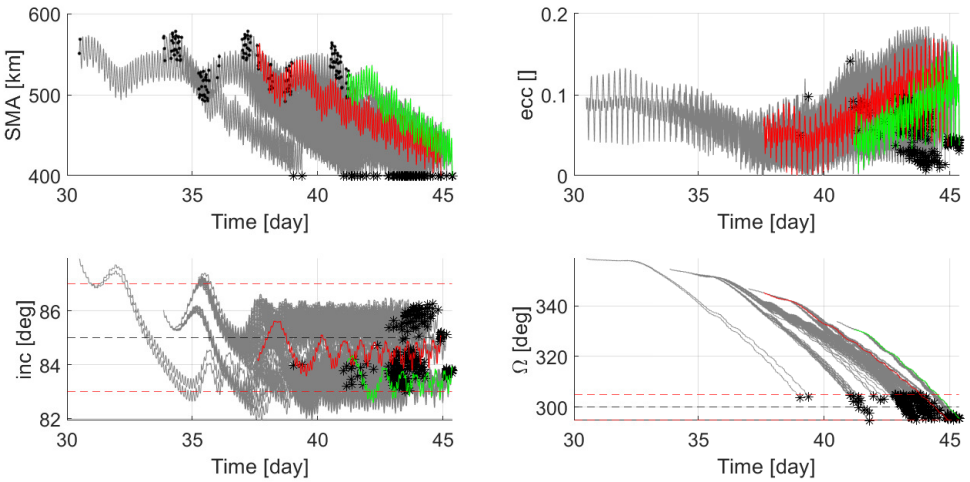

Figure 10: Propagation of the different solutions that satisfy the operational and geometrical constraints. In the upper left plot, the black points indicate the initial conditions. In all the plots the back stars represent the final values of each parameter at the end of the descent. In the lower plots, the desired final values of the inclination and Ω are represented by the black dashed lines and their respective tolerances are indicated by the two red dashed lines.

CONCLUSION

In this paper, the previous research on escape from 1:1 GTR is extended. A workflow for designing transfer orbits that utilize the gravitational perturbation from the 1:1 GTR during the approach phase is presented. The semimajor axis, inclination, and Ω are primarily affected by this resonance. Notably, the effect on the inclination can be systematically leveraged, as the inclination value remains nearly constant after the escape maneuver. The workflow uses a database of all possible solutions and a subset of it is chosen depending on the geometrical constraints, in terms of inclination and Ω, and the operational one, in terms of thrust magnitude. A case study utilizing this workflow is presented, and the final approach trajectory is obtained. In this trajectory, the optimization of the final value of the inclination is chosen, aiming to make it as close as possible to the desired value. Reducing maneuvers minimizes the inherent uncertainties associated with each course adjustment, thereby ensuring more accurate predictions of spacecraft state and trajectory. Therefore, implementing strategic mission planning, robust control mechanisms, and optimized flight paths that minimize the need for constant corrections is a beneficial approach. This strategy not only enhances mission reliability and success but also significantly contributes to the effective and efficient execution of space exploration initiatives. The utilization of the resonance is shown to facilitate, especially plane change maneuvers, resulting in cost savings for the mission.

ACKNOWLEDGEMENTS

This work is funded by ESA OSIP with the project title ”Resonance Capture of Low-Thrust Spacecraft Around a Small Body” and by the John Anderson Research Award Studentship.

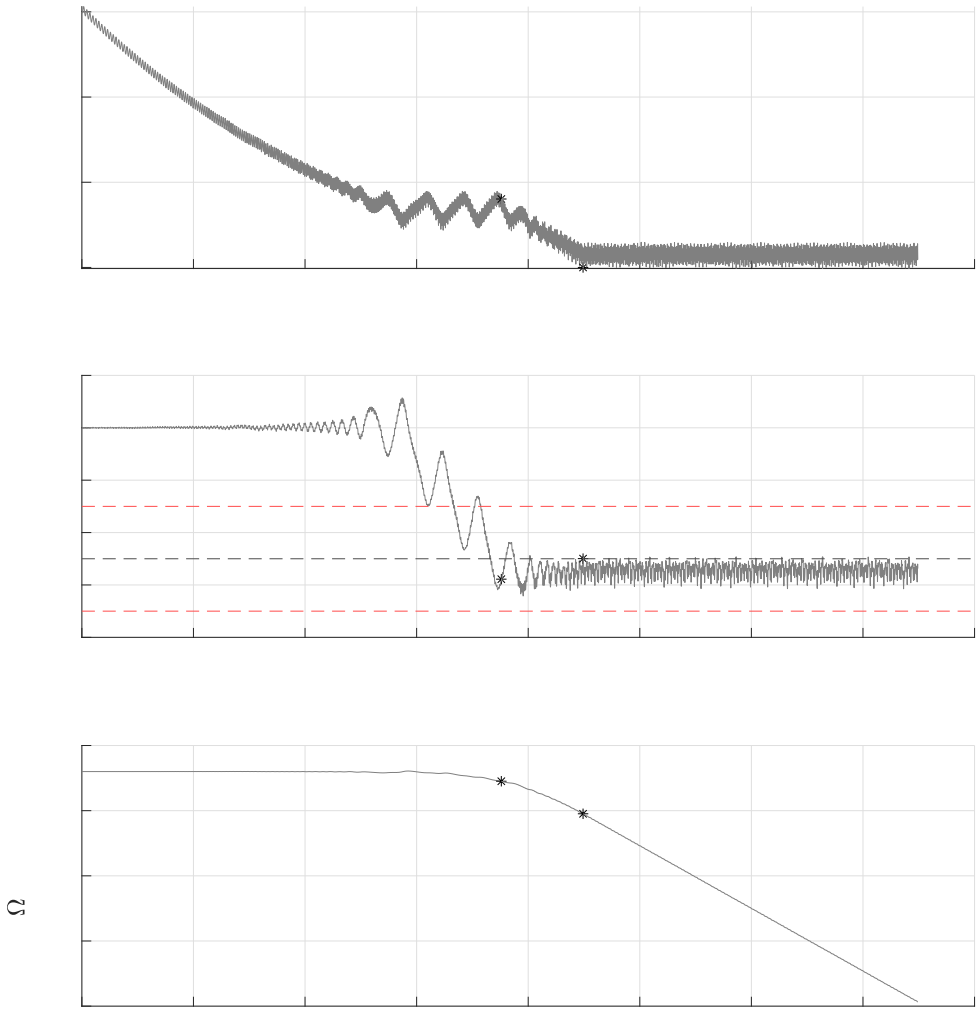

Figure 11: Orbital elements propagation of Dawn's complete descent trajectory.

REFERENCES

[1] A. Artemyev, A. Neishtadt, D. Vainchtein, A. Vasiliev, I. Vasko, and L. Zelenyi, "Trapping (capture) into resonance and scattering on resonance: Summary of results for space plasma systems," *Communications in Nonlinear Science and Numerical Simulation*, Vol. 65, 2018, pp. 111–160, 10.1016/j.cnsns.2018.05.004.

[2] B. Garfinkel, "On resonance in celestial mechanics," *Celestial Mechanics*, Vol. 28, 1982, pp. 275—-290, 10.1007/BF01243738.

[3] P. Tricarico and M. Sykes, "The Dynamical Environment of Dawn at Vesta," *Planetary and Space Science*, Vol. 58, 2010, pp. 1516–1525, 10.1016/j.pss.2010.07.017.

[4] C. Murray and S. Dermott, *Solar System Dynamics*. Cambridge University Press, 2000.

[5] A. Celletti, C. Gales, and C. Lhotka, "Resonances in the earth's space environment," *Communications in Nonlinear Science and Numerical Simulation*, Vol. 84, 2020, pp. 105—-185, 10.1016/j.cnsns.2020.105185.

[6] A. Lemaître, N. Delsate, and S. Valk, "A web of secondary resonances for large A/m geostationary debris," *Celestial Mechanics and Dynamical Astronomy*, Vol. 104, 2009, pp. 383—-402, 10.1007/s10569-009-9217-2.

[7] P. Goldreich and S. Peale, "Spin–orbit coupling in the Solar System," *Astronomical Journal*, Vol. 71, 1966, pp. 425—-438, 10.1086/109947.

[8] A. Celletti and C. Gales, "On the dynamics of space debris: 1:1 and 2:1 resonances," *J Nonlinear Sci*, Vol. 24, 2014, pp. 1231—-1262, 10.1007/s00332-014-9217-6.

[9] C. Russell, F. Capaccioni, A. Coradini, M. De Sanctis, W. Feldmann, R. Jaumann, H. Keller, T. Mccord, L. Mcfadden, S. Mottola, C. Pieters, T. Prettyman, C. Raymond, M. Sykes, D. Smtih, and M. Zuber, "Dawn Mission to Vesta and Ceres," *Earth, Moon and Planets*, Vol. 101, 2007, pp. 65–91, 10.1007/s11038-007-9151-9.

[10] N. Wallace, O. Sutherland, J. Bolter, H. Gray, A. Altay, F. Striedter, F. Budnik, S. Manganelli, E. Montagnon, and C. Steiger, "BepiColombo - Solar Electric Propulsion System Operations for the Transit to Mercury," 2019.

[11] K. Nishiyama, S. Hosoda, K. Ueno, R. Tsukizaki, and H. Kuninaka, "Development and Testing of the Hayabusa 2 Ion Engine System," *The Japan Society for Aeronautical and Space Sciences*, Vol. 14, 2016, pp. 131–140, 10.2322/tastj.14.Pb131.

[12] N. Delsate, "Analytical and numerical study of the ground-track resonances of Dawn orbiting Vesta," *Planetary and Space Science*, Vol. 59, 2012, 10.1016/j.pss.2011.04.013.

[13] G. Whiffen, "Optimal low-thrust orbital transfers around a rotating non-spherical body," *AAS/AIAA Space Flight Mechanics Meeting*, 2004.

[14] J. Feng, R. Noomen, X. Hou, P. Visser, and J. Yuan, "1:1 Ground-track resonance in a uniformly rotating 4th degree and order gravitational field," *Celestial Mechanics and Dynamical Astronomy*, Vol. 127, 2017, 10.1007/s10569-016-9717-9.

[15] O. Montenbruck and G. Eberhard, *Satellite Orbits - Models, Methods and Applications*, 10.1115/1.1451162.

[16] W. M. Kaula, *Theory of Satellite Geodesy: Applications of Satellites to Geodesy*. 1966.

[17] L. F. Shampine and M. K. Gordon, *Computer Solution of Ordinary Differential Equations: the Initial Value Problem*. San Francisco: W. H. Freeman, 1975.

[18] D. Scheeres, "The Effect of C22 on Orbit Energy and Angular Momentum," *Celestial Mechanics and Dynamical Astronomy*, Vol. 73, 1999, pp. 339—-348, 10.1023/A:1008384021964.

[19] S. Valk, A. Lemaître, and F. Deleflie, "Semi-analytical theory of mean orbital motion for geosynchronous space debris under gravitational influence," *Advances in Space Research*, Vol. 43, 2009, pp. 1070–1082, 10.1016/j.asr.2008.12.015.

[20] D. Boccaletti and G. Pucacco, *Theory of Orbits, Vol. 1: Integrable Systems and Non-perturbative Methods*. 2001.

[21] W. Boumchita and J. Feng, "Escape strategies from the capture into 1:1 resonance using low-thrust propulsion," *AAS/AIAA Space Flight Mechanics Meeting*, 2022.